Applied Catalysis B: Environmental 256 (2019) 117865

Contents lists available at ScienceDirect

Applied Catalysis B: Environmental

journal homepage: www.elsevier.com/locate/apcatb

A difunctional photocatalytic H_2 evolution composite co-catalyst tailored by integration with earth-abundant material and ultralow amount of noble metal

Baojun Ma*, Xin Li, Dekang Li, Keying Lin

State Key Laboratory of High-efficiency Coal Utilization and Green Chemical Engineering, College of Chemistry and Chemical Engineering, Ningxia University, Yinchuan, 750021, PR China

ARTICLE INFO

Keywords:
Composite co-catalyst
Noble metals
Earth-abundant materials
Molybdenum nitride
Photocatalytic hydrogen evolution

ABSTRACT

Noble metals and earth-abundant materials are two kinds of co-catalysts in photocatalytic hydrogen production. However, the profound roles and catalytic mechanisms between them need to be clarified. Here, we report a composite co-catalyst by integration with Mo_2N and Pt for efficient photocatalytic hydrogen production on CdS. Amazingly, the (Pt/Mo_2N) composite with ultralow amount of Pt (0.006%) shows most efficient. The activity of optimum (Pt / Mo_2N)/CdS reaches 1730 μmol/h/g, which are 6.2 times of Pt/CdS, 1.6 times of Mo_2N/CdS and 7.2 times sole CdS, respectively. Electrochemical tests demonstrate Mo_2N has large specific capacitance and mainly storing electrons, while Pt mainly acts as the catalytic active center. The different functions of Pt and Mo_2N account for the superiority of (Pt/Mo_2N). The fabrication strategy benefits the co-catalyst industrialization as both considerations to cost and efficiency.

1. Introduction

With the excessive consumptions of fossil fuels and consequent the environmental pollution problem, exploring new sustainable energy sources has become a constantly pursuing goal for the mankind. Photocatalytic hydrogen evolution on semiconductor photocatalysts using abundant solar energy has attracted much attention in recent decades, as it realizes the changes from solar energy to chemical energy (hydrogen energy) [1–10]. However, the ultralow activities of the bare photocatalysts greatly limit their industrialization in the future. Suitable co-catalyst decoration on the surface of semiconductor is an effective way to greatly promote the photocatalytic activity. Co-catalyst can provide catalytic sites and decrease the activation energy of the H_2 evolution reaction; facilitate the separation of the photo-excited charges in the semiconductor, hence increasing the photocatalytic efficiency [11–16].

The platinum group precious metal is a kind of famous co-catalyst with excellent performance for photocatalytic hydrogen evolution [17–20]. However, it is not suitable for industrialization because of the over-high cost. Recently, some earth-abundant and low cost co-catalysts [21–29] based Co, Mo, W elements and Graphene have been reported to substitute the noble-metals. Our group has also reported a series of molybdenum-based non-noble metal co-catalysts (MoP, Mo_2N, Mo_2C, Mo_2C/Mo_2N/GR) and summarizes their structures, kinds and roles in photocatalytic hydrogen evolution [30–34]. Most of molybdenum-based co-catalysts promote the hydrogen production and their co-catalytic performances are comparable to or even higher than the non-noble metals such as platinum. However, the difference between the noble metals and the non-noble metal co-catalysts, especially in the functions and roles are not completely clear to date. It should not be only focused on the non-noble metals co-catalysts while neglecting the noble metals. Generally, the noble metal with low Fermi energy and low over-potential has strong ability to catalyze protons reduction to produce hydrogen [9], while the non-noble metal co-catalyst not only has strong catalysis, but also more importantly, efficiently separates and transfers the charges in the semiconductor [35]. Taking advantage of both the earth-abundant co-catalyst and noble metal by integration with them to construct a composite co-catalyst, it is promising to obtain more efficient co-catalyst and deeper understanding of co-catalyst.

Here, we integrated non-noble metal co-catalyst Mo_2N and noble metal Pt to form a new composite co-catalyst (Pt/Mo_2N). After loading on the photocatalyst cadmium sulfide, the (Pt/Mo_2N) shows the most efficiently co-catalytic activity and the strong synergistic effects of Pt and Mo_2N. Most interestingly, the amount of Pt is ultralow (0.006%) with Mo_2N (2.0%) in the optimum photocatalyst (Pt/Mo_2N)/CdS, which means the low cost and high efficiency. The different roles of Pt

* Corresponding author.
E-mail address: bjma@nxu.edu.cn (B. Ma).

https://doi.org/10.1016/j.apcatb.2019.117865
Received 9 March 2019; Received in revised form 9 June 2019; Accepted 12 June 2019
Available online 13 June 2019

and Mo_2N are analyzed and demonstrated.

2. Experimental section

2.1. Preparation of Mo_2N and (Pt/Mo_2N)

All chemicals were of analytical grade and used without further purification and were obtained from Sinopharm Chemical Reagent Co., Ltd. (Beijing, China).

For preparing Mo_2N, 2.73 g ammonium heptamolybdate ($(NH_4)_6Mo_7O_{24}$•$4H_2O$) was put into the muffle furnace and calcined at 500 ℃ for 4 h in the air, then, the sample was reduced by temperature programmed reduction method for 4 h at 800 ℃ under flowing gas of NH_3 at a gas flow rate of 100 ml/min. The sample was rapidly cooled to room temperature in flowing gas of NH_3 and then passivated in mixed gas of N_2 and O_2 with the ratio of 99 for 12 h to form a stable material [31].

For the preparation of (Pt/Mo_2N), the impregnation method was adopted. Briefly, different amount of aqueous solution of Pt (0.037 mg/mL) using H_2PtCl_6•$6H_2O$ as Pt precursor were impregnated on the surface of Mo_2N (0.2 g), then, the samples were reduced in the H_2 flow of 100 ml/min at 300 ℃ for 1 h.

2.2. Preparation of CdS, Mo_2N / CdS, (Pt / Mo_2N)/CdS and Pt / CdS

CdS was synthesized by precipitation method [31]. Detailly, 50 ml of 0.14 mol/L of cadmium acetate solution was used as reaction reagent. Then, 60 ml of 0.14 mol/L of Na_2S solution was added dropwise under vigorous agitation and then aged for 12 h. Last, the deposit was filtered by distilled water and ethanol several times and then dried at 60 ℃ for 12 h in vacuum drying oven.

The Mo_2N/CdS and (Pt/Mo_2N)/CdS were prepared by coprecipitation method [31]. Here, the loading amount of Mo_2N was 2.0% both in Mo_2N / CdS and (Pt/Mo_2N)/CdS. For the preparation of Mo_2N/CdS, except 0.02 g of Mo_2N was dispersed in 50 ml of 0.14 mol/L of cadmium acetate solution. Other steps were same as the method of preparation of CdS. For the preparation of (Pt / Mo_2N) / CdS, (Pt / Mo_2N) with different loading amount of Pt was used as additive. Except 0.02 g of (Pt/Mo_2N) was dispersed in 50 ml of 0.14 mol/L of cadmium acetate solution, other steps were same as the method of preparation of CdS.

The Pt/CdS was prepared by in situ photodeposition method [31]. Briefly, different amount of aqueous solution of Pt (0.037 mg/mL) using H_2PtCl_6•$6H_2O$ as Pt precursor were impregnated on the surface of 0.1 g of CdS by in situ photodeposition method using 10% lactic acid aqueous solution (100 mL) as holes scavenger and 300 W Xe lamp (Perfect, China) with 420 nm filter ($\lambda \geq 420$ nm) as light resource. After 1 h of photocatalytic reaction, the deposit was filtered by distilled water and ethanol several times and then dried at 60 ℃ for 12 h in vacuum drying oven. The photocatalytic reaction conditions are same as that test of photocatalytic H_2 evolution.

2.3. Characterizations of co-catalysts and photocatalysts

The structures of co-catalysts and photocatalysts were determined by X-ray diffractometry (D / MAX2500, Rigaku, Japan) at room temperature at a voltage of 4 kV under Cu-K_α radiation. The UV/Vis diffuse reflection spectroscopies (UV–vis DRS) were recorded by a spectrometer (U-4100) with $BaSO_4$ used for the corrected base line. High resolution transmission electron microscopy (HRTEM) and TEM images were taken on a transmission electron microscope (F20) equipped with an energy-dispersive X-ray analyser. The X-ray photoelectron spectra (XPS) data were obtained on a Thermo ESCALAB 250Xi spectrometer using Al Kα as the irradiation source (hν = 1486.6 eV, 150 W).

2.4. The photocatalytic H2 evolution

The photocatalytic hydrogen evolution experiments were performed in a closed system (Perfect, China) of evacuation and gas circulation with a quartz cell. A 300 W Xe lamp (Perfect, China) with a 420 nm filter was used as visible light source. In detail, 0.1 g of sample was dispersed in an aqueous solution (100 mL) containing 10 ml lactic acid. The reaction system was pumped to vacuum for 30 min before irradiation, and the temperature of the reaction solutions was always kept at room temperature by using cooling water during the reaction. The hydrogen gas was analyzed by an online gas chromatographic equipped with a 5 Å molecular sieve column and TCD detector, using Ar as the carrier gas.

2.5. Electrochemical and photoelectrochemical measurements

Electrochemical and photoelectrochemical performances of the samples were studied on a CHI 760D electrochemical work station (Shanghai Chenhua Instrument Co., Ltd, Shanghai, China) in a standard three-electrode system with the sample-coated FTO or foam Ni film as the working electrode, a SCE (saturated calomel electrode) as a reference electrode, and a Pt sheet as the counter electrode. The photocurrent responses were studied under 300 W Xe lamp with 420 nm filter. 0.5 M Na_2SO_4 solution was used as the electrolyte.

Electrochemical impedance spectroscopies, linear sweep voltammetry, and transient photocurrent responses of the samples were studied using the sample-coated FTO film as the working electrode [36] except that of Pt cocatalyst was used commercial Pt sheet.

Specific capacitance performances (Cyclic voltammetry) of the samples were carried out using the sample-coated foam Ni as the working electrode [37]. The specific capacitance is calculated according the formula of $C = \frac{\int IdV}{v\Delta E}$, Where C (F) is the total capacitance, $\int IdV$ is the areas of close curves, ΔE (V) is the electrochemical window, v (V / s) is the scanning rate [38].

3. Results and discussion

3.1. The physical structures and properties of composite co-catalysts (Pt / Mo_2N)

Fig. 1 shows the XRD patterns of different co-catalysts and

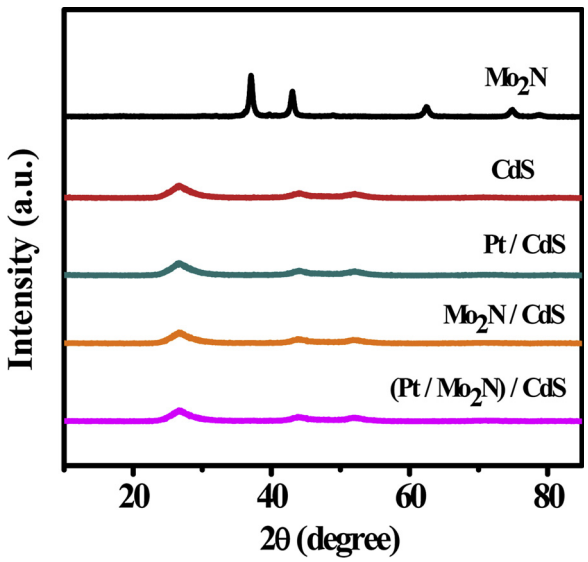

Fig. 1. XRD patterns of different samples. The loading amount of Mo_2N both in Mo_2N/CdS and (Pt/Mo_2N)/CdS is 2.0%. The loading amount of Pt both in Pt/CdS and (Pt / Mo_2N)/CdS is 0.006%.

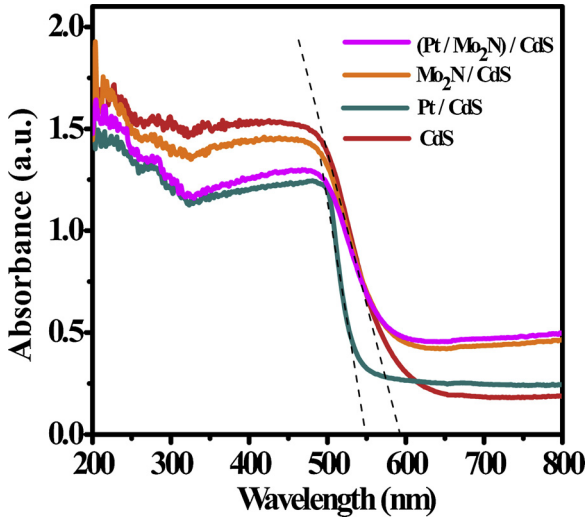

Fig. 2. UV–vis diffuse reflection spectroscopies of different samples. The loading amount of Mo_2N both in Mo_2N/CdS and (Pt/Mo_2N)/CdS is 2.0%. The loading amount of Pt both in Pt/CdS and (Pt/Mo_2N)/CdS is 0.006%.

photocatalysts. It can be seen the Mo_2N is in accordance to that of JCPDS#25-1366 and the CdS is in accordance to that of JCPDS#10-0454, which indicates the Mo_2N and CdS were successfully synthesized. However, the Pt / CdS, Mo_2N / CdS and (Pt / Mo_2N) / CdS show the same patterns as the CdS, it is because the loading amount of Mo_2N (2.0%) or Pt (0.006%) is much low. The ultralow amount of co-catalyst is beneficial to the whole cost of a photocatalyst, especially for precious metal co-catalyst.

Fig. 2 shows UV–vis diffuse reflection spectroscopy of bare CdS and CdS loaded with different co-catalysts. The bare CdS with the onset of absorption edge of 593 nm shows the band gap of 2.09 eV. Comparing with the bare CdS, the Mo_2N/CdS and (Pt/Mo_2N)/CdS show an enhanced photoabsorption in visible light region, while the Pt/CdS shows an apparently shift towards short wavelength indicating a wider band gap of CdS in Pt/CdS. The wider band gap of CdS in Pt/CdS is attributed to the enhanced crytallinity of CdS caused by the two times of desiccation of CdS during the in situ photo-impregnation of Pt on CdS.

To demonstrate the successful preparation of composite co-catalyst (Pt/Mo_2N), the TEM images of (0.3% Pt/Mo_2N) are shown in Fig. 3. It is clearly seen some tiny dots with the diameter of about 1.0 nm are located on the surface of Mo_2N. The tiny dots are Pt particles. The lattice

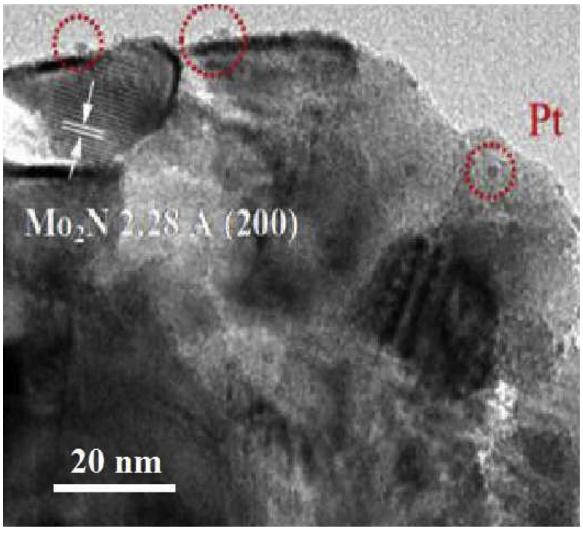

Fig. 3. TEM images of Pt / Mo_2N. The loading amount of Pt in Pt/Mo_2N is 0.3%.

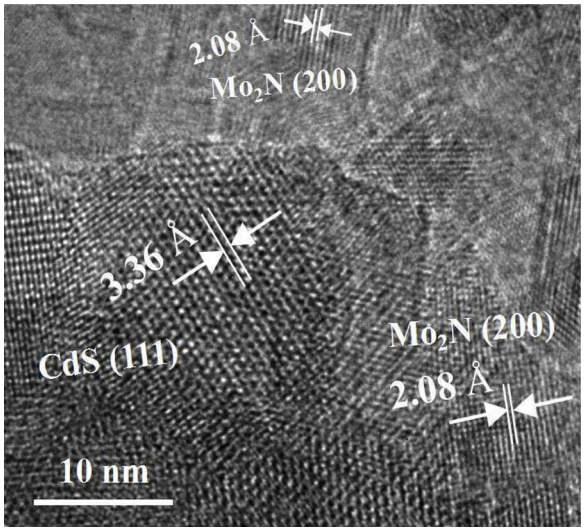

Fig. 4. The HRTEM images of Mo_2N/CdS. The loading amount of Mo_2N in Mo_2N/CdS is 2.0%.

fringes of Mo_2N with interplanar distances of 0.228 nm is indexed to the (200) planes of Mo_2N.

Fig. 4 shows the HRTEM images of 2.0% Mo_2N/CdS. The lattice fringes of Mo_2N with interplanar distances of 0.228 nm is indexed to the (200) planes of Mo_2N, while the lattice fringes of CdS with interplanar distances of 0.336 nm is indexed to the (111) planes of CdS, respectively. The HRTEM images of (0.006% Pt/2.0% Mo_2N)/CdS had also been carried out, however, it is basically similar to that of 2.0% Mo_2N/CdS, and the Pt particles cannot be found due to its ultralow amount. The EDS-mappings of (0.006% Pt/2.0% Mo_2N) / CdS are also implemented as shown in Fig. S1, it can be seen that the Mo and N elements are evenly dispersed on the surface of CdS. However, the Pt element is not be distinguished by the EDS-mapping due to the ultralow loading amount of Pt (0.006%).

Fig. 5 shows the XPS of (0.006% Pt/2.0% Mo_2N)/CdS. The peaks of Cd (Fig. 5a) at 405.2 and 412.0 eV are the Cd $3d_{5/2}$ and Cd $3d_{3/2}$ of Cd^{2+}, and the peaks of S (Fig. 5b) at 161.3 and 162.5 eV are the S $2p_{3/2}$ and S $2p_{1/2}$ of S^{2-} [39]. The peaks of Mo (Fig. 5c) at 228.4 and 231.7 eV are the Mo $3d_{5/2}$ and Mo $3d_{3/2}$ of Mo^{2+}, and the peak observed at 226 eV is ascribed to S 2 s [40]. The peak at 405.0 eV is ascribed to N 1s. The peaks of Pt (Fig. 5e) at 69.4 and 75.3 eV are associated with the Pt $4f_{5/2}$ and Pt $4f_{7/2}$ of Pt^0 [41], which indicates the successfully loading of Pt. The XPS of CdS, 0.006% Pt/CdS, 2.0% Mo_2N/CdS were shown in Fig. S2.

3.2. Photocatalytic H_2 evolution on CdS loaded with composite co-catalyst (Pt / Mo_2N)

To evaluate the co-catalytic property of the composite co-catalyst (Pt/Mo_2N), photocatalytic H_2 evolution on CdS loaded with different co-catalysts are shown in Fig. 6. The CdS alone shows much low photocatalytic H_2 evolution activities of 240 μmol/h/g. when CdS is loaded with co-catalysts, the photocatalytic activities are improved largely, whatever the co-catalysts are Pt, Mo_2N or (Pt/Mo_2N). It indicates all the Pt, Mo_2N and (Pt/Mo_2N) are effective co-catalysts for photocatalytic H_2 evolution. Here, the loading amount of Mo_2N is adopted the optimal 2.0% [31]. Amazingly, when the noble metal Pt and earth abundant Mo_2N integrate to form a new composite co-catalyst (Pt / Mo_2N), the composite co-catalyst (Pt/Mo_2N) shows the largest co-catalytic H_2 evolution activity at the ultralow amount of 0.006% Pt. The activity of optimum (Pt/Mo_2N)/CdS reaches 1730 μmol/h/g, which are 6.2 times of Pt / CdS (280 μmol/h/g), 1.6 times of Mo_2N/CdS (1080 μmol/h/g) and 7.2 times sole CdS (240 μmol/h/g), respectively. The **co**-catalytic

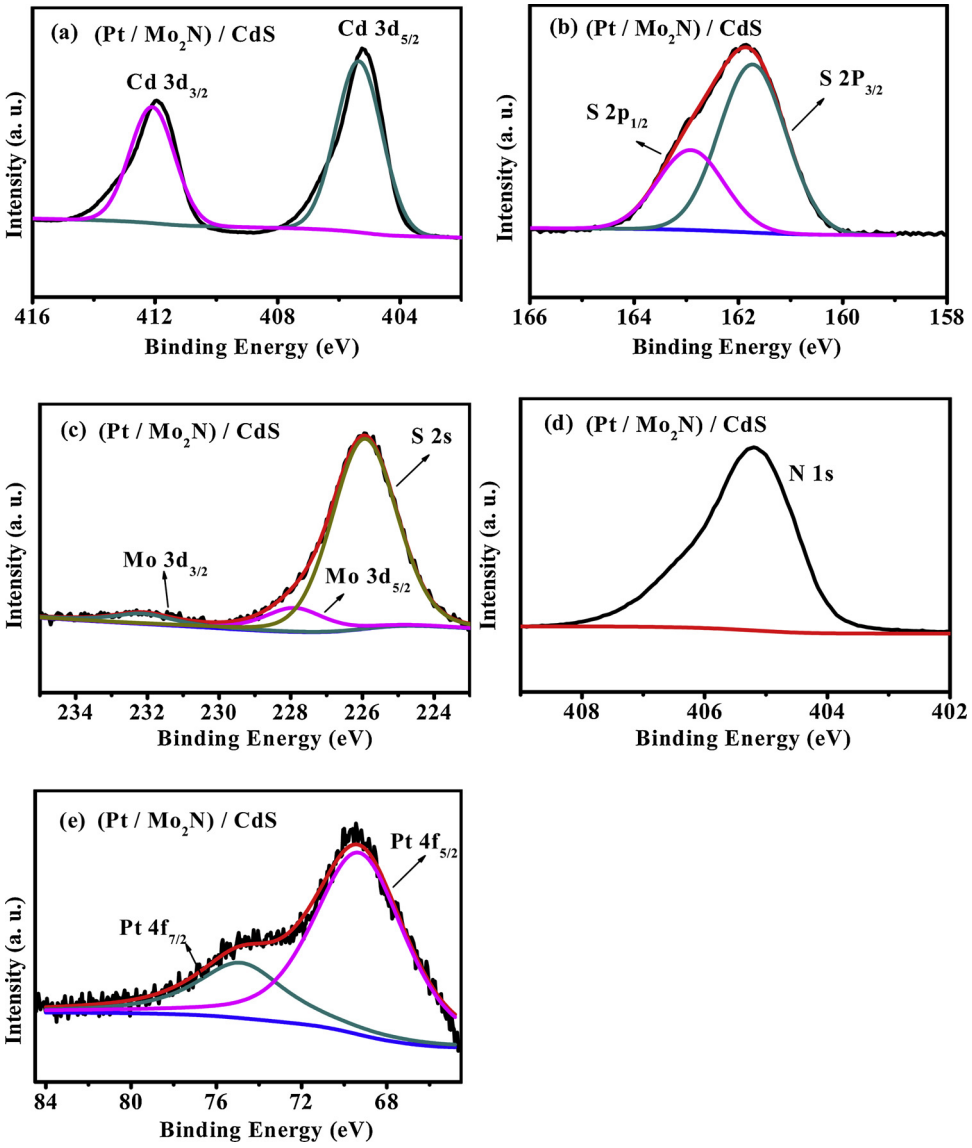

Fig. 5. The XPS of (0.006% Pt / 2.0% Mo_2N)/CdS (a–e).

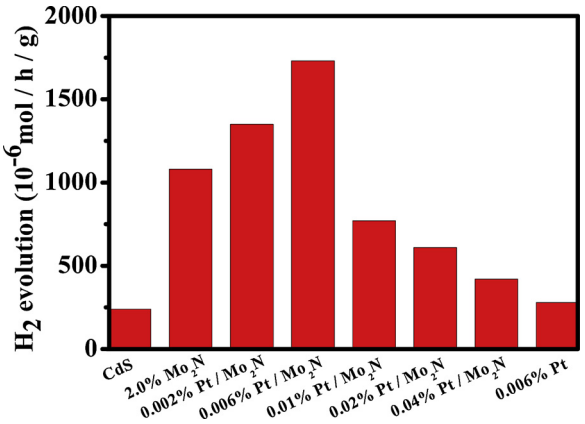

Fig. 6. Photocatalytic H_2 evolution on CdS loaded with different co-catalysts. In the (Pt/Mo_2N)/CdS samples, all the amount of Mo_2N is 2.0%. Reaction condition: 0.1 g catalyst; 300 W Xe lamp with 420 nm filter.

effect of the composite (Pt / Mo_2N) is even higher than that of the sum of sole Pt and sole Mo_2N, which shows the synergistic **co-**catalytic effect of Pt and Mo_2N. It means the Pt and Mo_2N in the composite (Pt/Mo_2N) interact each other or play different roles for photocatalytic H_2 evolution. The stability of CdS loaded with the hybrid co-catalyst can maintain more than two days (Fig. S3). A comparative table (Table S1) of H_2 production rate with different co-catalysts was also presented. This new hybrid co-catalyst Pt / Mo_2N shows much improvement of catalytic activities compared with Pt alone and Mo_2N alone. Pt / Mo_2N is in medium level among all reported co-catalysts. It is lower than some co-catalysts (GQDs, Mo_2N/Mo_2C/graphene, Ti_3C_2, Pt_3Co), it is due to the different base material for co-catalysts. It also means this fabrication strategy of hybrid co-catalyst (electron storage material with proton catalysis material) has the broader prospects for development.

3.3. Electrochemical and photoelectrochemical performances of composite cocatalyst (Pt/Mo_2N)

Fig. 7 shows the electrochemical impedance spectra of different sample electrodes. The Pt co-catalyst shows a typical metal property with no semicircles which means the strong electron conduction ability.

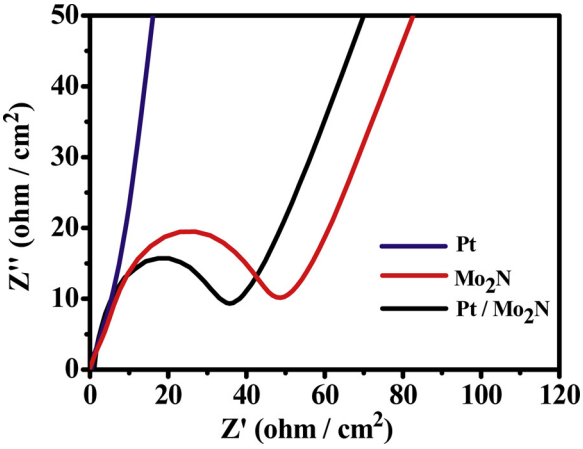

Fig. 7. Electrochemical impedance spectra of different co-catalysts. The loading amount of Pt in Pt / Mo_2N is 0.3%. The electrochemical impedance spectra of Pt is directly gained from the commercial Pt sheet.

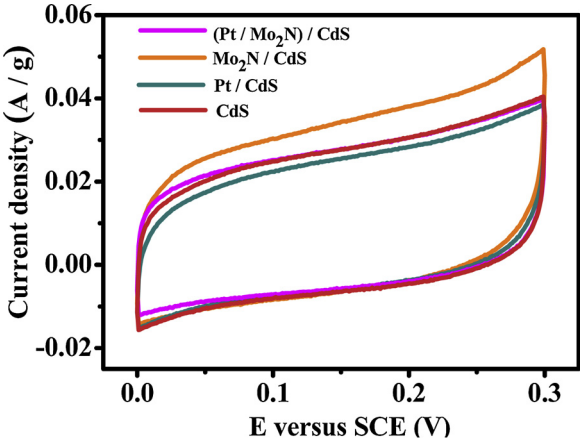

Fig. 9. Cyclic voltammetry curves of CdS loaded with different co-catalysts. The loading amount of Mo_2N both in Mo_2N/CdS and (Pt/Mo_2N)/CdS is 2.0%. The loading amount of Pt both in Pt/CdS and (Pt/Mo_2N)/CdS is 0.006%.

Mo_2N and (Pt/Mo_2N) show similar electrochemical impedance spectra except the different semi-diameter of semicircles. The smaller semicircle of (Pt/Mo_2N) than that of Mo_2N alone means the stronger electron conduction ability of (Pt/Mo_2N) due to integration of Mo_2N with the noble metal of Pt.

Fig. 8 shows the linear sweep voltammetry curves for different co-catalysts. Apparently, the Pt shows the lowest over-potential for H_2 evolution which means the strongest electro-catalytic ability for proton reduction. Comparing the Mo_2N and (Pt/Mo_2N), the over-potential of the (Pt/Mo_2N) becomes lower due to the integration of Mo_2N with the noble metal of Pt. Combination of Figs. 7 and 8, the stronger electron conduction ability and the lower over-potential of composite co-catalysts (Pt/Mo_2N) are in favor of the electro-catalytic H_2 evolution compared with Mo_2N alone due to the introduction of the well-known superior electro-catalyst Pt.

Fig. 9 shows the cyclic voltammetry curves of CdS loaded with different **co**-catalysts. The CdS alone has area enclosed by the cyclic voltammetry curve which is corresponding to its specific capacitance of the 650.6 m F/g. Loading Mo_2N on CdS, the Mo_2N / CdS shows the largest areas enclosed by the cyclic voltammetry curves which means the largest specific capacitance (762.6 m F/g). However, when the noble metal Pt loaded on CdS, the Pt/CdS shows the smallest area and the smallest specific capacitance (582.6 m F/g). The (Pt / Mo_2N)/CdS shows almost equal area and specific capacitance (639.4 m F/g) of CdS alone, which is due to the positive effect of Mo_2N and negative effect of Pt for the specific capacitance. According to the Figs. 7 and 8, the Pt has the superior electro-catalysis to the Mo_2N. However, the Mo_2N/CdS shows the higher photocatalytic H_2 activity than the Pt/CdS (Fig. 6) [31], this indicates Mo_2N plays another role besides the electro-catalysis in the photocatalysis. The Mo_2N with the enhanced specific capacitance is in favor of storing photoelectrons from excited CdS as a reservoir, thus improving the separation of photo-charges in CdS, and finally enhancing the whole photocatalytic efficiency of CdS. With regard to the composite co-catalyst (Pt/Mo_2N), it not only possesses the super electro-catalytic ability of Pt, but also has the electron storing ability of Mo_2N, thus shows the synergistic effect of Pt and Mo_2N and the largest photocatalytic H_2 evolution activity on CdS.

Fig. 10 shows the transient photocurrent responses of CdS loaded with different co-catalysts, the sole CdS is also presented for comparison.

Compared with CdS alone, all the photocurrents are obviously

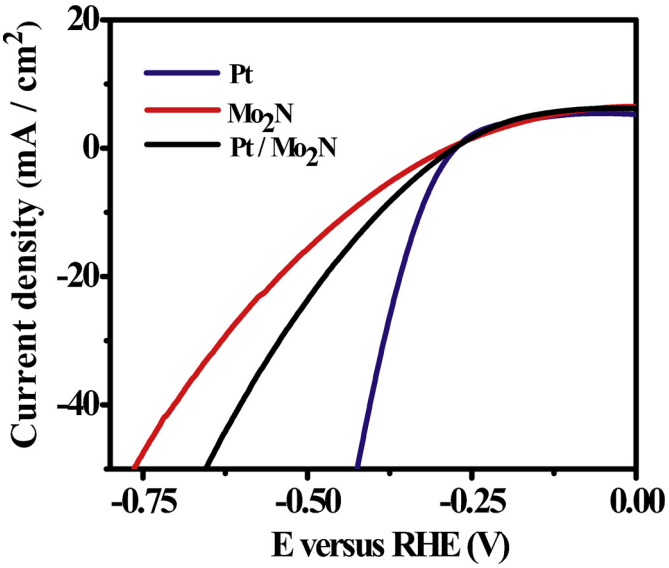

Fig. 8. Linear sweep voltammetry curves of different co-catalysts. The loading amount of Pt in Pt / Mo_2N is 0.3%. The linear sweep voltammetry curves of Pt is directly gained from the commercial Pt sheet.

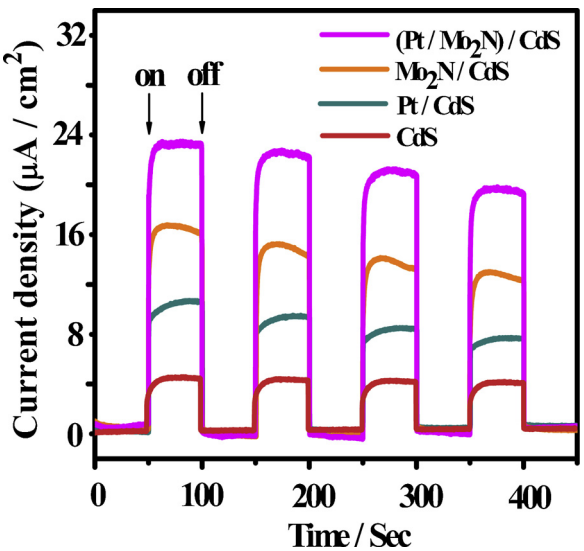

Fig. 10. Transient photocurrent responses of different samples. The loading amount of Mo_2N both in Mo_2N/CdS and (Pt/Mo_2N)/CdS is 2.0%. The loading amount of Pt both in Pt/CdS and (Pt/Mo_2N)/CdS is 0.006%.

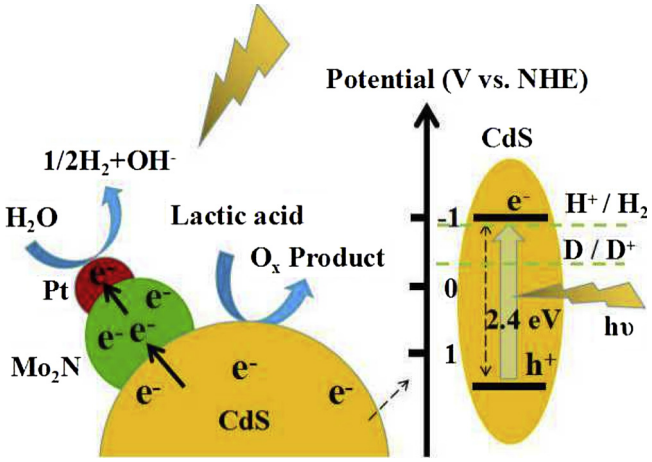

Fig. 11. The mechanism of photocatalytic H_2 evolution on (Pt/Mo_2N)/CdS.

enhanced, when the CdS is loading with co-catalysts. The (Pt/Mo_2N)/CdS shows the largest photocurrent, which is corresponding to the largest photocatalytic activity, further demonstrating the superiority of the composite co-catalyst (Pt / Mo_2N).

3.4. The roles and mechanism of composite co-catalyst (Pt / Mo_2N) for photocatalytic H_2 evolution on CdS

Fig. 11 shows the mechanism of photocatalytic H_2 evolution on (Pt/Mo_2N)/CdS photocatalysts. The Mo_2N with ultralow amount of Pt is loaded on the surface of CdS to form a photocatalyst. Here, the Mo_2N and Pt together integrate to form a composite cocatalyst Pt/Mo_2N. Under visible light irradiation, the photo-excited holes in valence band of CdS can oxidize the lactic acid to the oxides of lactic acid. The photoexcited electrons in conduction band of CdS can be injected into Mo_2N which may act as a reservoir of electrons due to its large specific capacitance. The Mo_2N with large specific capacitance improves the separation and inhibits the combination of the photo-excited charges in CdS, thus enhances the photocatalytic efficiency of CdS. When there is some Pt on the Mo_2N, the elections collected and stored by the Mo_2N will rapidly catalyze and reduce the protons to form hydrogen molecular through the Pt due to the low over-potential and strong election conduction ability of Pt, thus further enhances the whole photocatalytic H_2 evolution activity of CdS. The roles of storing electrons of the Mo_2N and the catalysis of Pt together account for the greatly enhanced photocatalytic activity of (Pt/Mo_2N)/CdS.

4. Conclusion

In summary, here, we reported a new composite co-catalyst (Pt/Mo_2N) by integration with earth-abundant material Mo_2N and noble metal Pt for efficient photocatalytic H_2 evolution. The activity of optimum (Pt/Mo_2N)/CdS reaches 1730 μmol/h/g, which are 6.2 times of Pt/CdS, 1.6 times of Mo_2N/CdS and 7.2 times sole CdS, respectively. The composite **co**-catalyst (Pt / Mo_2N) is given consideration to both efficiency and cost due to the ultralow (0.006%) loading amount of Pt. The roles of Mo_2N and Pt are clarified. The Mo_2N mainly acts as a reservoir to collect and store photo-excited electrons from CdS due to its large specific capacitance, while the Pt mainly acts as the catalytic active center for proton reduction. The different functions of the Pt and Mo_2N both account for the superiority of (Pt/Mo_2N). This study presents a new idea to fabricate both efficient and low cost co-catalytst (composite co-catalyst) for photocatalytic H_2 evolution by integration with earth-abundant material and ultralow amount of noble metal.

Acknowledgements

This work is funded by the National First-rate Discipline Construction Project of Ningxia (Chemical Engineering and Technology), Project of Key Research Plan of Ningxia (2019BDE03003), Major Innovation Projects for Building First-class Universities in China's Western Region (ZKZD2017003), and the National Natural Science Foundation of China (NSFC, 21862014).

Appendix A. Supplementary data

Supplementary material related to this article can be found, in the online version, at doi:https://doi.org/10.1016/j.apcatb.2019.117865.

References

[1] X.B. Chen, S.H. Shen, L.J. Guo, S.S. Mao, Chem. Rev. 110 (2010) 6503–6570.
[2] T. Hisatomi, J. Kubota, K. Domen, Chem. Soc. Rev. 43 (2014) 7520–7535.
[3] W.Y. Wang, H. Wang, Q.J. Zhu, W. Qin, G.Y. Han, J.R. Shen, X. Zong, C. Li, Angew. Chem. Int. Ed. 55 (2016) 9229–9233.
[4] C.S. Pan, J. Xu, Y.J. Wang, D. Li, Y.F. Zhu, Adv. Funct. Mater. 22 (2012) 1518–1524.
[5] L.W. Zhang, Y. Man, Y.F. Zhu, ACS Catal. 1 (2011) 841–848.
[6] Q. Li, B.D. Guo, J.G. Yu, J.G. Ran, B.H. Zhang, H.J. Yan, J.R. Gong, J. Am. Chem. Soc. 133 (2011) 10878–10884.
[7] B.J. Ma, F.Y. Wen, H.F. Jiang, J.H. Yang, P.L. Ying, C. Li, Catal. Lett. 134 (2010) 78–86.
[8] H.F. Zhang, Z. Yang, W. Yu, H. Wang, W.G. Ma, X. Zong, C. Li, Adv. Energy Mater. 8 (2018) 1800795.
[9] X.M. Wang, H. Wang, H.F. Zhang, W. Yu, X.L. Wang, Y. Zhao, X. Zong, C. Li, ACS Energy Lett. 3 (5) (2018) 1159–1164.
[10] Z.L. Wang, J.F. Han, Z. Li, M.R. Li, H. Wang, X. Zong, C. Li, Adv. Energy Mater. 6 (2016) 1600864.
[11] J.H. Yang, D.E. Wang, H.X. Han, C. Li, Acc. Chem. Res. 46 (2013) 1900–1909.
[12] K. Chang, X. Hai, J.H. Ye, Adv. Energy Mater. 6 (2016) 1502555.
[13] Q.J. Xiang, J.G. Yu, M. Jaroniec, J. Am. Chem. Soc. 134 (2012) 6575–6578.
[14] H. Wang, X.M. Wang, R.T. Chen, H.F. Zhang, X.L. Wang, J.H. Wang, J. Zhang, L.C. Mu, K.F. Wu, F.T. Fan, X. Zong, C. Li, ACS Energy Lett. 4 (1) (2019) 40–47.
[15] G. Yang, H. Ding, D.M. Chen, J.J. Feng, Q. Hao, Y.F. Zhu, Appl. Catal. B: Environ. 234 (2018) 260–267.
[16] X.J. Bai, L. Wang, Y.F. Zhu, ACS Catal. 2 (2012) 2769–2778.
[17] H.J. Yan, J.H. Yang, G.J. Ma, G.P. Wu, X. Zong, Z.B. Lei, J.Y. Shi, C. Li, J. Catal. 266 (2009) 165–168.
[18] Y. Ma, Q. Xu, X. Zong, D.E. Wang, G.P. Wu, X. Wang, C. Li, Energy Environ. Sci. 5 (2012) 6345–6351.
[19] J.G. Yu, L.F. Qi, M. Jaroniec, J. Phys. Chem. C 114 (2010) 13118–13125.
[20] B.J. Ma, J.S. Kim, C.H. Choi, S.I. Woo, Int. J. Hydrogen Energy 38 (2013) 3582–3587.
[21] D.M. Chen, J.J. Yang, Y. Zhu, Y.M. Zhang, Y.F. Zhu, Appl. Catal. B: Environ. 233 (5) (2018) 202–212.
[22] Q. Guo, F. Liang, X.Y. Gao, Q.C. Gan, X.B. Li, J. Li, Z.H. Lin, C.H. Tung, L.Z. Wu, ACS Catal. 8 (7) (2018) 5890–5895.
[23] Z.F. Huang, J.J. Song, X. Wang, L. Pan, K. Li, X.W. Zhang, L. Wang, J.J. Zou, Nano Energy 40 (2017) 308–316.
[24] B. Tian, W.L. Zhen, H.B. Gao, X.Q. Zhang, Z. Li, G.X. Lu, Appl. Catal. B: Environ. 203 (2017) 789–797.
[25] L. Guo, Z. Yang, K. Marcus, Z. Li, B. Luo, L. Zhou, X. Wang, Y. Du, Y. Yang, Energy Environ. Sci. 11 (2018) 106–114.
[26] D.F. Xu, B. Cheng, W.K. Wang, C.J. Jiang, J.G. Yu, Appl. Catal. B: Environ. 231 (2018) 368–380.
[27] Q.J. Xiang, J.G. Yu, M. Jaroniec, J. Phys. Chem. C. 115 (2011) 7355–7363.
[28] J.J. Yang, D.M. Chen, Y. Zhu, Y.M. Zhang, Y.F. Zhu, Appl. Catal. B: Environ. 205 (2017) 228–237.
[29] X.K. Zeng, Z.Y. Wang, G. Wang, T.R. Gengenbach, D.T. McCarthy, A. Deletic, J.G. Yu, X.W. Zhang, Appl. Catal. B: Environ. 218 (2017) 163–173.
[30] B.J. Ma, R.S. Zhang, K.Y. Lin, H.X. Liu, X.Y. Wang, W.Y. Liu, H.J. Zhan, Chinese J. Catal. 39 (2018) 527–533.
[31] B.J. Ma, Y.H. Liu, J. Li, K.Y. Lin, H.X. Liu, X.Y. Wang, W.Y. Liu, H.J. Zhan, Int. J. Hydrogen Energy 41 (2016) 22009–22016.
[32] B.J. Ma, H.J. Xu, K.Y. Lin, J. Li, H.J. Zhan, W.Y. Liu, C. Li, ChemSusChem 9 (2016) 820–824.
[33] B.J. Ma, X.Y. Wang, K.Y. Lin, J. Li, Y.H. Liu, H.J. Zhan, W.Y. Liu, Int. J. Hydrogen Energy 42 (2017) 18977–18984.
[34] B.J. Ma, D.K. Li, X.Y. Wang, K.Y. Lin, ChemSusChem 11 (2018) 3871–3881.
[35] J.R. Ran, J. Zhang, J.G. Yu, M. Jaroniecc, S.Z. Qiao, Chem. Soc. Rev. 43 (2014) 7787–7812.
[36] Y.S. Fu, X.Y. Gao, D.S. Zha, J.W. Zhu, X.P. Ouyang, X. Wang, J. Mater. Chem. 6 (2018) 1601–1611.
[37] F.S. Wu, X.H. Wang, W.R. zheng, H.W. Gao, C.H. Hao, C.W. Ge, Electrochim. Acta 245 (2017) 685–695.
[38] J.E. Li, Y.W. Wang, W.N. Xu, Y. Wang, B. Zhang, S. Luo, X.Y. Zhou, C.L. Zhang,

X. Gu, C.G. Hu, Nano Energy 57 (2019) 379–387.
[39] T.M. Di, B.C. Zhu, J. Zhang, B. Cheng, J.G. Yu, Appl. Surf. Sci. 389 (2016) 775–782.
[40] J. Feng, C.H. An, L.X. Dai, J.X. Liu, G.J. Wei, S. Bai, J. Zhang, Y.J. Xiong, Chem. Eng. J. 283 (2016) 351–357.
[41] B. Han, S.Q. Liu, N. Zhang, Y.J. Xu, Z.R. Tang, Appl. Catal. B: Environ. 202 (2017) 298–304.